ŁUKASZ KUKOŁOWICZ[1, 2, *]
ORCID: 0000-0002-9984-8700

DARIUSZ OLESZAK[2]
ORCID: 0000-0002-7563-007X

[1] Baker Hughes, al. Krakowska 110/114, 02-256 Warsaw, Poland

[2] Warsaw University of Technology, Faculty of Materials Science and Engineering, Wołoska 141, 02-507 Warsaw, Poland

* Corresponding author

DOI: 10.15199/40.2023.2.1

Influence of anisotropy of mechanical properties on hydrogen induced cracking

Wpływ anizotropii właściwości mechanicznych na podatność na pękanie wodorowe

Hydrogen induced cracking is a form of wet H_2S cracking. Blistering or crack propagation is a result of the mechanical tearing of material by high-pressure hydrogen gas forming on internal material discontinuities, like non-metallic inclusions. This failure mechanism is typically associated with low and medium-strength pipeline steels, however, it does also occur in high-strength rolled wire. This evaluation aims to elucidate the mechanism of this susceptibility. The characteristic failure pattern where cracking occurs near the wire centreline and propagates perpendicular to the rolling direction leads to believe that the wire anisotropy, developed during cold rolling, plays a critical role. A mechanical property – flow resistance in principal directions – was measured using the Wheeler and Ireland technique. It was found that the "weak" direction is perpendicular to the crack propagation direction. The failure rate does not correspond to the flow resistance, but rather to the flow resistance ratios. It is proposed that those ratios are not only a measure of anisotropy but also a measure of microstructural damage inflicted by the cold rolling process. This microstructural damage is partially reversible by heat treatment processes.

Keywords: hydrogen induced cracking, flow resistance, anisotropy, cold rolled wire

Pękanie wodorowe jest mechanizmem degradacji często zachodzącym w środowiskach korozyjnych, w których występuje siarkowodór. Propagacja pęknięć postępuje na skutek fizycznego rozrywania materiału przez cząsteczkowy wodór pod wysokim ciśnieniem, tworzący się na nieciągłościach wewnętrznych, takich jak na przykład wtrącenia niemetaliczne. Praca badawcza dotyczy mechanizmu pękania wysoko wytrzymałego kształtowego drutu stalowego. Drut pęka w charakterystyczny sposób: pęknięcie tworzy się w pobliżu środka drutu i propaguje równolegle do płaskich powierzchni. Obserwacja ta każe przypuszczać, że propagacja związana jest z anizotropią właściwości mechanicznych drutu. Anizotropię zbadano jako opór płynięcia plastycznego materiału pod wgłębnikiem twardościomierza metodą Wheelera i Irelanda. Zaobserwowano, że pęknięcia propagują prostopadle do kierunku, w którym występuje najmniejszy opór płynięcia. Pękanie podczas testów w środowisku korozyjnym z siarkowodorem nie jest skorelowane bezpośrednio z oporem płynięcia, a ze stosunkiem oporów płynięcia w dwu kierunkach, a więc miarą anizotropii. Z badań wynika, że proces walcowania na zimno powoduje uszkodzenia mikrostruktury, które można szacować miarą anizotropii właściwości mechanicznych drutu i które są częściowo odwracalne w procesie obróbki cieplnej.

Słowa kluczowe: kolumna destylacji atmosferycznej ropy naftowej, korozja górnej części kolumny atmosferycznej, hydroliza chlorków organicznych i nieorganicznych

1. Introduction

Rolled wire is used, among others, in the construction of unbonded flexible pipe to API 17J [1] standard used for subsea and offshore developments. The flattened shape allows for tighter packing of steel layers. In this application corrosive gasses, including H_2S, can diffuse through a polymer barrier. As such, the standard requires a wire resistant to degradation mechanisms caused by this environment, in particular, to Hydrogen Induced Cracking (HIC) and Sulphide Stress Cracking (SSC). This investigation focuses on Cold Rolled (CR) wires which failed sour

Łukasz Kukołowicz, MSc Eng. Graduate from the Faculty of Materials Science and Engineering of the Warsaw University of Technology. Since 2011 employee of GE O&G, now after the merger Baker Hughes. Main areas of interest are corrosion and hydrogen embrittlement of metallic materials, large forgings, failure analysis with over 90 analyses carried out to date. The topic of the PhD work is an analysis of the sour service test failures of the cold rolled wires.
E-mail: lukasz.kukolowicz.dokt@pw.edu.pl, lukasz.kukolowicz@bakerhughes.com

Dariusz Oleszak, DSc, PhD, Eng., Professor at the Faculty of Materials Science and Engineering, WUT. Research area includes manufacturing, microstructure and properties of metallic materials.
E-mail: dariusz.oleszak@pw.edu.pl

Otrzymano / Received: 28.11.2022. Przyjęto / Accepted: 23.01.2023

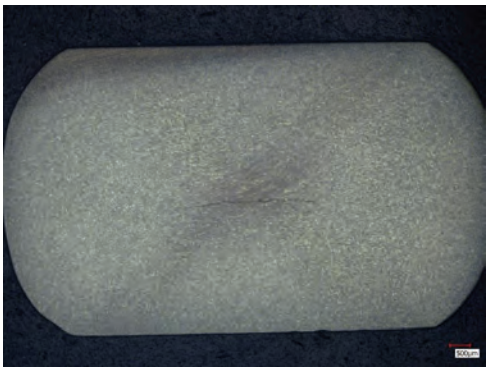

Fig. 1. An example of wire cross-section etched with Nital with a HIC near the centreline. Etching reveals a "X" pattern near diagonals related to plastic deformation during the cold rolling process

Rys. 1. Przykładowy zgład ujawniający pęknięcie wodorowe w pobliżu osi drutu, trawiony Nitalem. Trawienie ujawnia wzór „X" między przekątnymi profilu, związany z procesem walcowania na zimno

testing by HIC. HIC is typically associated with low-strength pipeline steels and it seldomly occurs for X80 and higher-strength pipeline steels with UTS above 700 MPa. ASM Handbook [2] defines it as "the cracking in low-to medium-strength steels in the absence of applied stress where the driving force for crack propagation is molecular hydrogen pressure build-up within the crack". High strength steels are naturally more resistant to this degradation mechanism. In rolled wires, HIC occurs near the centreline and propagates perpendicular to the wire width as shown in Fig. 1. This pattern indicates the existence of an easy crack propagation path.

Majority of the publications on the flexible pipe wires focus on a corrosion behaviour primarily iron supersaturation and H_2S consumption [3]. When testing is performed in conditions replicating the annulus, there is a beneficial effect of very low H_2S additions reducing the corrosion rate [4, 5], as compared to pure CO_2. However, the acetic ions present in NACE TM0177 solution B prevent formation of the protective scale thus the acceptance testing is much more aggressive than the field conditions.

The flow surface was determined by the technique by Lee and Backofen [6], based on Wheeler and Ireland approach [7, 8]. The technique analyses the stress state under the indent as a sum of hydrostatic pressure and shear stress. The deviatoric stresses are defined as:

$$\begin{aligned} s_1 &= \sigma_1 - \sigma, \\ s_2 &= \sigma_2 - \sigma, \\ s_3 &= \sigma_3 - \sigma, \end{aligned} \tag{1}$$

where σ_1, σ_2, σ_3 are the principal stress and σ is the hydrostatic stress given as (2):

$$\sigma = \frac{1}{3}(\sigma_1 + \sigma_2 + \sigma_3). \tag{2}$$

For plane strain conditions Huber-Mises-Hencky hypothesis correlates flow surface to the stress state as (3):

$$KHN \approx (\sigma_1{}^2 - \sigma_1\sigma_2 + \sigma_2{}^2)^{\frac{1}{2}}. \tag{3}$$

This can be transposed to (4):

$$\sigma_i \approx KHN \cdot (1 - \alpha_i + \alpha_i{}^2)^{-\frac{1}{2}}. \tag{4}$$

The material flow surface is constructed from the six KHN values obtained from the indentations made along two directions of each of the three orthogonal planes of material's principal axes. The weights a, depend on the indentation diagonals ratio δ. For the Knoop indent it is approximately 7 : 1. The values of a for each indent orientation a–f and are given as (5):

$$\begin{aligned} \alpha_a &= \frac{\sigma_2}{\sigma_1} = (2+\delta)/(2\delta+1), \\ \alpha_b &= \frac{1}{\alpha_a}, \\ \alpha_c &= (1-\delta)(2+\delta), \\ \alpha_d &= (\delta-1)(1+2\delta), \\ \alpha_e &= \frac{1}{\alpha_d}, \\ \alpha_f &= \frac{1}{\alpha_c}. \end{aligned} \tag{5}$$

Each indent on the flow surface has two coordinates $[[KHN \cdot (1-\alpha_i+\alpha_i{}^2)^{-\frac{1}{2}}; \alpha_i \cdot KHN \cdot (1-\alpha_i+\alpha_i{}^2)^{-\frac{1}{2}}]$. Determination of the plastic flow properties in Z-Y plane was achieved by rotation. In practical terms the new order of indents is d, c, b, a, f, e.

2. Experimental procedures

2.1. Material

The wires for this evaluation were high-carbon steels. Among the 16 samples tested (A–P) there were three wire grades:

- SR: 861–1034 MPa UTS cold rolled and stress relieved 0.60–0.65% C (3 samples),
- TE: 1310–1482 MPa UTS cold rolled and tempered 0.65–0.75% C (1 sample),
- CR: 1310–1482 MPa UTS cold rolled 0.60–0.70% C (12 samples).

Cold rolling of hot rolled wire with ultrafine pearlitic microstructure was carried out in a way that the total reduction of wire cross-section was about 50% for all wire grades. The wire profile final dimensions varied from 9 × 3 to 12 × 7 mm. The stress-relieving process was carried out in a hydrogen protective atmosphere at about 400°C for a few hours. The wire grade TE was subject to a rapid recovery heat treatment [9]. The recovery heat treatment consisted of rapid heating to above 600°C, hold time was below 5 seconds, and was followed by rapid cooling.

2.2. General microstructure evaluation

The general microstructure of tensile wire was revealed by etching with 5% ammonium persulfate $(NH_4)_2S_2O_8$ with addition of 0.05% EDTA in water. Etching time 5–20 seconds. Observations were carried out using Leica DM4000 M LED at 500× optical magnification.

2.3. Experimental procedure

Samples were prepared by cutting each wire sample in three perpendicular planes intersecting the wire centreline, mounting in resin, grounding, and polishing. Knoop hardness was measured using LECO LV 700AT at 10 kG load in 6 orientations marked 'a' to 'f'. The cutting plan, indentation orientations, and markings are shown in Fig. 2.

Two indentations were performed in each of the six orientations. The average of the two was subsequently used for the calculation of points along the KHN flow resistance surface. An example of the flow resistance surface representation of sample P is shown in Fig. 3.

2.4. Sour service testing

Tests consisted of 30-day immersion testing of five samples pre-stressed by four points bending to 0.5% total elongation in outer fibres. The testing solution was NACE TM0177 modified to contain 3.5% NaCl, saturated and continuously bubbled with a gas mixture of H_2S and CO_2 at atmospheric pressure. The partial pressure of H_2S within the gas mixture was up to 1 mbar. After the test samples were subject to a visual and magnetic particle inspection, followed by ultrasonic testing and microscopic inspection of sectioned wire.

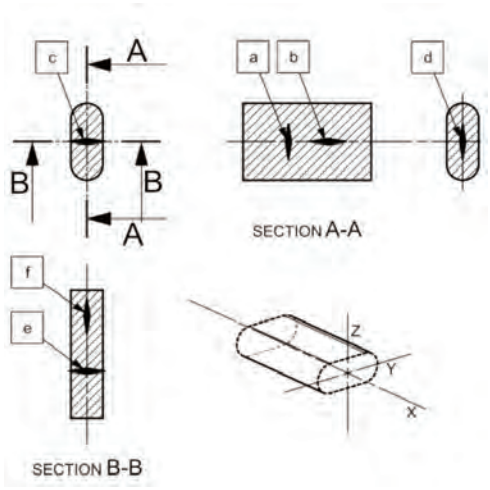

Fig. 2. Wire-cutting plans and Knoop indentation orientations (letters in boxes indicate the indent identification letter); principal axis naming is shown in the isometric view

Rys. 2. Plan cięcia i orientacje wgłębnika (oznaczone literami w prostokątach); główne kierunki zaznaczono w rzucie izometrycznym

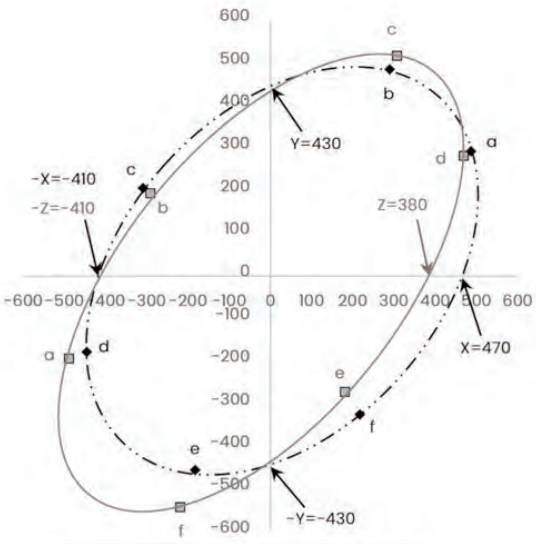

Fig. 3. Plane intersections of the flow resistance surface of sample P: black – intersection with the X-Y plane, grey – intersection with the Z-Y plane; the values of the flow resistance in the principal directions are the intersection points with the coordinate system axis

Rys. 3. Przecięcie powierzchni oporu plastycznego płynięcia z płaszczyznami dla próbki P: czarna przerywana linia – przecięcie z płaszczyzną X-Y, szara ciągła linia – przecięcie z płaszczyzną Z-Y; wartości oporu plastycznego płynięcia w głównych kierunkach oznaczono jako punkty przecięcia z osiami układu współrzędnych

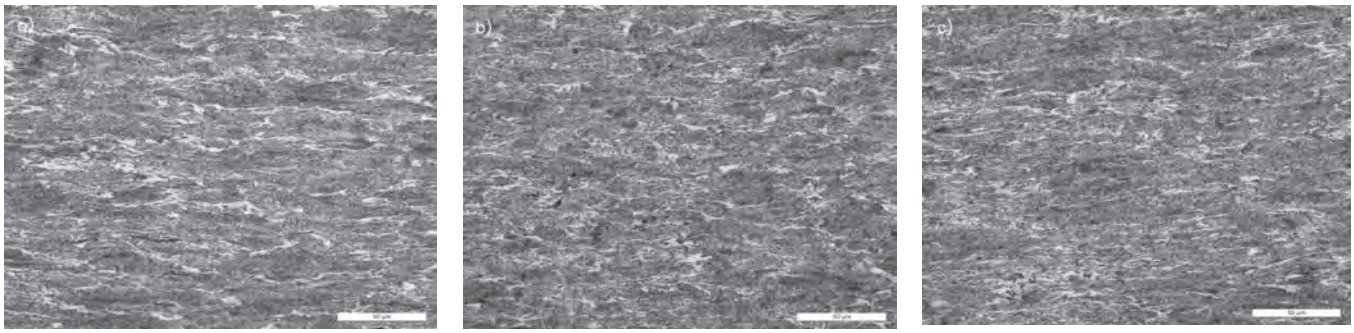

Fig. 4. General microstructure of wire grade SR: a) microstructure in Z-X plane, ¼ wire thickness above the centreline; b) microstructure in Y-Z plane, ¼ wire thickness above the centreline; c) microstructure in Z-X plane, near the centreline

Rys. 4. Mikrostruktura drutu SR: a) mikrostruktura w płaszczyźnie Z-X, ¼ grubości drutu nad osią drutu; b) mikrostruktura w płaszczyźnie Y-Z, ¼ grubości drutu nad osią drutu; c) mikrostruktura w płaszczyźnie Y-Z, w osi drutu

2.5. Microstructure evaluation of centreline segregation

A retrospective microstructure analysis was carried out to determine the source of the measurement error inconsistency. The following etching procedure was used to reveal centreline segregation in CR wire grade:

1. Electrolytic etch in 20% KOH saturated with picric acid at 8V for 40 s.
2. 0.5% Nital 3–5 s.
3. 40 ml glycerin (waterless), 3 ml HNO_3, 6 ml HF 5–10 s.

For SR and TE wire grades using the third step of the procedure was sufficient. Additional microhardness tests at 300 gf load were carried out using a Zwick ZHVμ hardness tester.

3. Results

3.1. General microstructure

The microstructure of sample A is representative for wire grade SR. The microstructure is pearlitic-ferritic with partial spheroidization of pearlite. The grains are axially elongated as shown in Fig. 4a. The microstructure is deformed also in the width direction. The deformation in the centreline is greater that in ¼ thickness location as shown in Fig. 4c and 4b, respectively.

The microstructure of sample D, wire grade TE consists of fine partially spheroidized pearlite. The elongation along the wire axis is evidenced in Fig. 5a. Width wise deformation of grains is relatively small in ¼ thickness location but becomes evident near the centreline as shown in Fig. 5b and 5c, respectively.

The microstructure of sample L, representative of wire grade CR consists of fine pearlite and allotriomorphic ferrite. The elongation along the wire axis is evidenced in Fig. 6a. Width wise deformation of grains is negligible in ¼ thickness location but becomes evident near the centreline as shown in Fig. 6b and 6c, respectively. A part of the centreline segregation region with lower deformation and with reduced ferrite content is visible at the top of the later picture.

3.2. Hardness measurement error

The measurement error was normalized by expressing each measurement error as a percentage deviation from the average KHN hardness measured for each wire sample and each orientation. The standard deviation of normalized measurements was calculated for each indent orientation. The standard deviation was multiplied by the *t*-Student value for 95% confidence and presented in Table 1 as the measurement error.

It was found that a significant measurement error was observed for indent orientation d. The etching of samples after indentation revealed a dark etching region interpreted as a centreline segregation from the continuous casting process. In some samples,

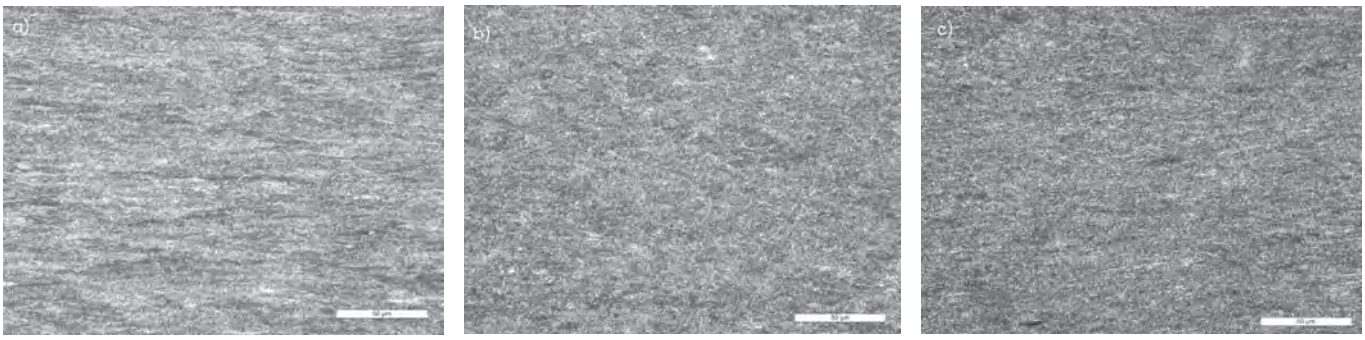

Fig. 5. General microstructure of wire grade TE: a) microstructure in Z-X plane, ¼ wire thickness above the centreline; b) microstructure in Y-Z plane, ¼ wire thickness above the centreline; c) microstructure in Z-X plane, near the centreline

Rys. 5. Mikrostruktura drutu TE: a) mikrostruktura w płaszczyźnie Z-X, ¼ grubości drutu nad osią drutu; b) mikrostruktura w płaszczyźnie Y-Z, ¼ grubości drutu nad osią drutu; c) mikrostruktura w płaszczyźnie Y-Z, w osi drutu

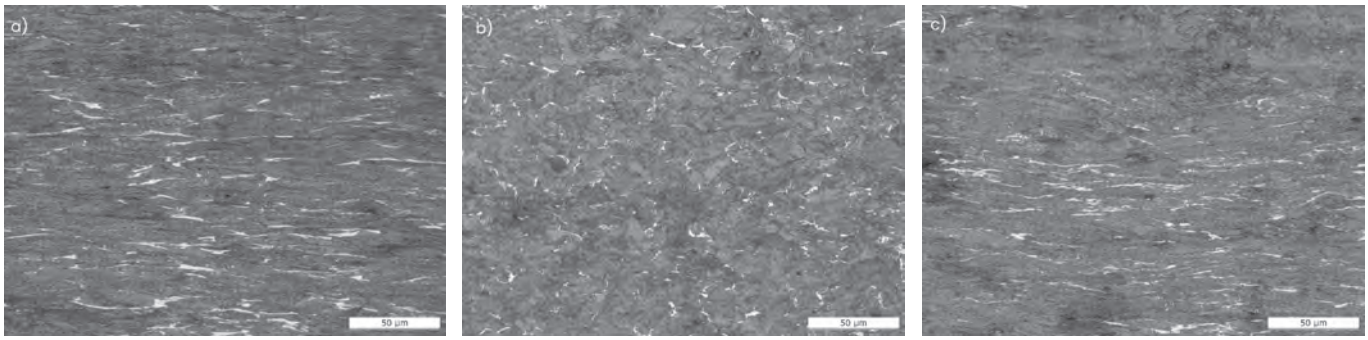

Fig. 6. General microstructure of wire grade CR: a) microstructure in Z-X plane, ¼ wire thickness above the centreline; b) microstructure in Y-Z plane, ¼ wire thickness above the centreline; c) microstructure in Z-X plane, near the centreline

Rys. 6. Mikrostruktura drutu CR: a) mikrostruktura w płaszczyźnie Z-X, ¼ grubości drutu nad osią drutu; b) mikrostruktura w płaszczyźnie Y-Z, ¼ grubości drutu nad osią drutu; c) mikrostruktura w płaszczyźnie Y-Z, w osi drutu

Table 1. Normalized measurement error for Knoop hardness in each orientation
Tabela 1. Znormalizowany błąd pomiaru twardości Knoopa dla każdej orientacji wgłębnika

Orientation	a	b	c	d	e	f
Measurement error [%]	±1.0	±1.3	±1.3	±4.3	±1.7	±0.8

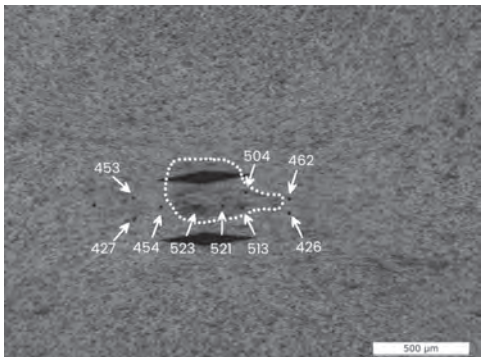

Fig. 7. Microstructure evaluation of sample P (the centreline segregation is outlined in white dotted line); Knoop indents are in orientation d; microhardness survey shows Vickers HV0.3 results

Rys. 7. Mikrostruktura próbki P trawiona w celu ujawnienia segregacji powstałej podczas odlewania (obszar segregacji zakreślono białą kropkowaną linią); odciski twardości Knoopa w orientacji d; na rysunek naniesiono wyniki pomiarów mikrotwardości HV0.3

Table 2. Summary of flow resistance in tension and compression in principal directions and failure rate in a sour test
Tabela 2. Zestawienie wyników oporu plastycznego płynięcia w głównych kierunkach rozciągania i ściskania

Sample ID	Grade	Size [mm]	X [KHN]	–X [KHN]	Y [KHN]	–Y [KHN]	Z [KHN]	–Z [KHN]	Failure rate
A	SR	9 × 3	320	–300	320	–320	290	–300	0
B	SR	12 × 4	320	–300	310	–310	290	–300	0
C	SR	12 × 4	310	–300	320	–320	280	–300	0
D	TE	12 × 7	400	–400	400	–400	380	–400	0
E	CR	9 × 3	440	–440	460	–430	340	–390	1.0
F	CR	10 × 5	460	–380	400	–450	360	–400	0.2
G	CR	10 × 5	480	–420	410	–410	370	–370	0.6
H	CR	10 × 5	430	–400	400	–400	340	–360	0.2
I	CR	12 × 4	420	–380	420	–370	330	–400	0.4
J	CR	12 × 6	460	–440	440	–440	360	–440	0.6
K	CR	12 × 6	480	–420	420	–420	380	–400	0.2
L	CR	12 × 6	460	–420	415	–460	415	–415	0.0
M	CR	12 × 7	420	–390	400	–390	380	–410	0.2
N	CR	12 × 7	480	–420	440	–420	370	–420	0.4
O	CR	12 × 7	500	–420	440	–440	360	–430	0.8
P	CR	12 × 7	470	–410	430	–430	380	–410	0.6

the segregation region was off-centre and did not interfere with Knoop hardness indents. An example of microstructure in sample P is shown in a photograph in Fig. 7. The centreline segregation was outlined in magenta for visibility and was about 500 µm wide and 300 µm high. Microhardness evaluation showed elevated hardness within this region, up to 523 HV10, compared to 426–462 HV10 in the microstructural region adjacent to it.

3.3. Flow resistance and sour service performance

The flow resistance in tension and compression in primary directions is summarized in Table 2 along with a normalized

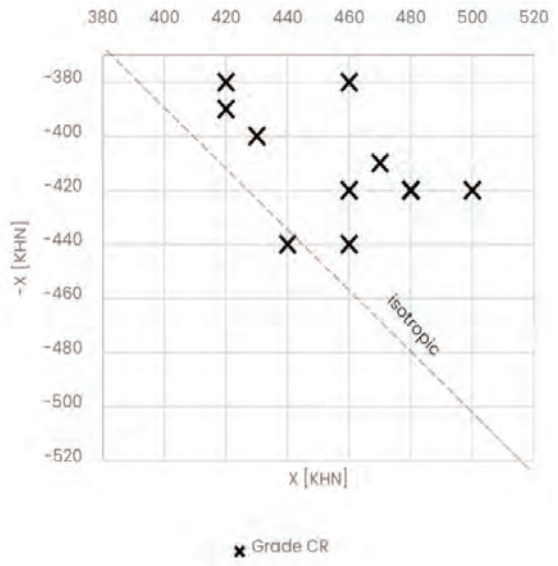

Fig. 8. Plot of the flow resistance X and –X for grade CR

Rys. 8. Wykres oporu plastycznego płynięcia w kierunku X: rozciągania (X) i ściskania (–X) dla drutu CR

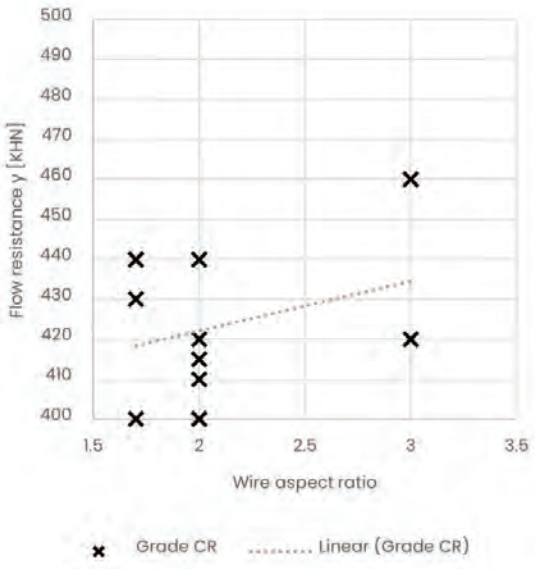

Fig. 10. Plot of the flow resistance Y and the wire aspect ratio – the flow resistance appears to increase with the increasing wire aspect ratio

Rys. 10. Opór plastycznego płynięcia i kierunku Y wykazuje korelację z proporcjami przekroju drutu

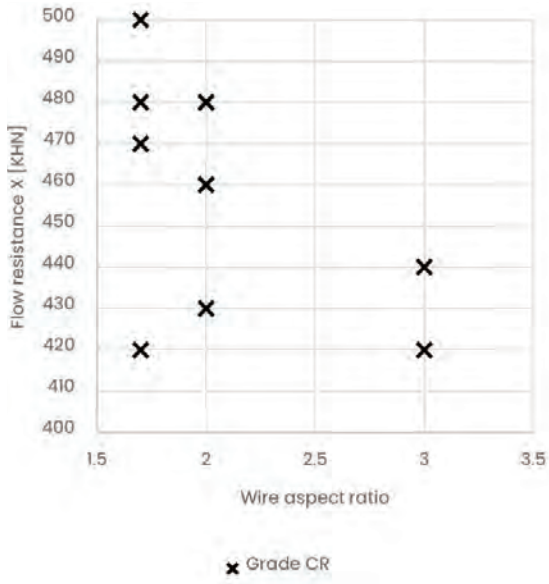

Fig. 9. Plot of the flow resistance X and the wire aspect ratio – no correlation between the two variables

Rys. 9. Opór plastycznego płynięcia i kierunku X nie wykazuje korelacji z proporcjami przekroju drutu

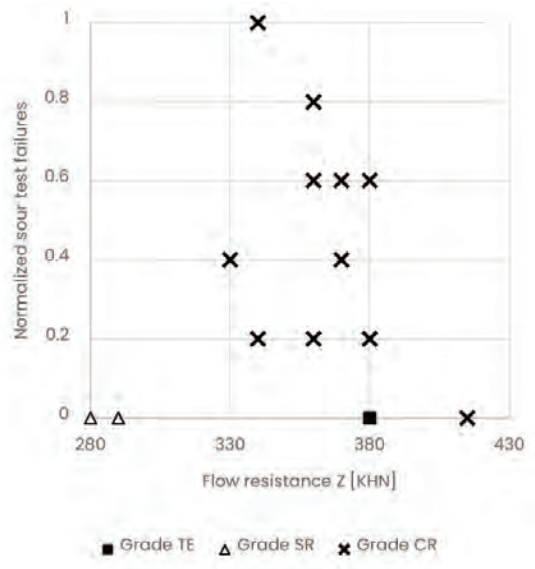

Fig. 11. Plot of the flow resistance Z and the normalized sour test result showing no correlation for the CR grade wire

Rys. 11. Opór plastycznego płynięcia i kierunku Z nie wykazuje korelacji ze znormalizowanym wynikiem testów korozyjnych drutu CR

sample failure rate. In the convention of this paper, compression is indicated by a minus sign. All sour test failures were caused by HIC.

All wire grades were shown to be anisotropic. It was found that flow resistance in the Z direction is the lowest for all wires. Wire grade TE was the least anisotropic showing 5% lower flow resistance in the Z direction than in the X direction, 380 and 400 KHN respectively. For wire SR the average flow resistance in the Z direction is 287 KHN, while the average flow resistance in the X direction is 317 KHN; a 10% reduction. For grade CR the average flow resistance in the Z direction was 366 KHN, while the average in the X direction was 460 KHN; a 20% reduction.

The flow resistance in the X direction should correspond to the tensile strength limits for the given wire grade:

$$UTS = \frac{1}{3} \cdot KHN \cdot 9.81. \quad (6)$$

For grade SR the measured flow resistances 310–320 KHN were within the expected 263–326 KHN range. For grade TE, the measured flow resistance of 400 KHN was within the expected 400–453 KHN range. For grade CR, the measured flow resistances 420 to 500 KHN were higher than the minimum expected 400 KHN, but 8 out of 12 samples exceeded the maximum expected value of 453 KHN.

For most samples of grade CR, the tensile flow resistance in the X direction was significantly higher than the compression flow resistance, as shown in Fig. 8. It seems that the wire aspect ratio, defined as the wire profile width to height, does not affect the centreline flow resistance in the X direction, as shown in Fig. 9.

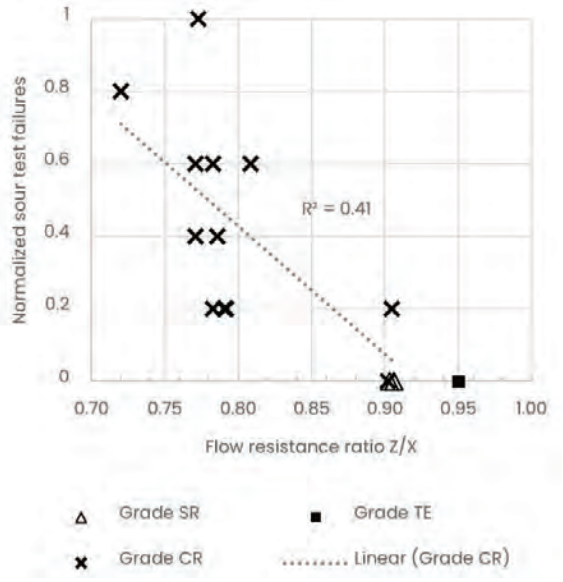

Fig. 12. Plot of the flow resistance ratio Z/X and the normalized sour test result showing an inverse correlation

Rys. 12. Korelacja wyników testów korozyjnych drutu CR ze stosunkiem oporów płynięcia w kierunkach Z i X

The flow resistance in the Y direction was higher than in the Z direction for all samples tested. In two cases the flow resistance in the Y direction was higher than in the X direction. On average for wire grade, CR flow resistance in the Y direction was 422 KHN; an 8% reduction from the average flow resistance in the X direction. The flow resistance in the Y direction appears to increase with the increasing aspect ratio, as shown in Fig. 10.

Statistical tests showed no correlation between the failure rate and the flow resistance in any principal direction for the wire grade CR. An example of the flow resistance in the Z direction plotted against the failure rate is shown in Fig. 11. A linear trend for improved sour resistance of grade CR was observed with the increasing flow resistance ratio Z/X, as shown in Fig. 12.

4. Discussion

Analysis of the measurement errors shows they are acceptable. The other successful use of Wheeler and Ireland technique reported in the literature by Ankamma [10] were applied to the materials with a uniform distribution of chemical composition and cold work. The authors carried out 15 measurements in each orientation using 100 gf load. The resulting measurement error up to 5% is comparable with the one obtained in this work. For the wire material the measurement error can be further reduced by etching samples to reveal the segregation and then placing indents outside of the centreline segregated region.

The measured flow resistance in the X direction corresponds well with the expected tensile strength of wire grades SR and TE. The performed evaluation was insufficient to perform validation of the Wheeler and Ireland technique for rolled wires. Especially after the flow resistance of grade CR turned out to be higher than expected. It may be of future interest to correlate the KHN flow resistance with the results of micro-tensile tests.

The measured flow resistance supports the hypothesis that the Z direction is a "weak" direction and thus an easy path for HIC propagation. The flow resistance in the Z direction does not statistically correlate with the failure rate. However, as a measure of anisotropy, the ratio of the flow resistances Z/X does show an inverse correlation with the failure rate.

The findings of this investigation point toward a hypothesis that Z/X anisotropy is a measure of damage accumulation within the wire centreline. It can be speculated that this damage is of the type that can be reversed by heat treatment. HIC propagation occurs not only by mechanical tearing of material in a weak direction but by more complex interaction which includes the factor of microstructural damage.

There seem to be other independent variables responsible for the wide spread of measured data points. It can be speculated that controlling those factors would allow CR wire grade to limit damage accumulation and decrease the failure rate.

5. Conclusions

The following can be concluded from this investigation:

- The microstructure of all wire grades is deformed axially and width wise, the highest deformation was observed near the centreline.
- The Wheeler and Ireland technique proved useful in evaluating the anisotropy of rolled wires.
- Measured flow resistance in the X direction corresponds well with wire UTS for grades SR and TE.
- Majority of measurement errors came from indents in orientation d. There is a potential to improve the technique described therein by avoiding placing indents in the centreline segregation region.
- All wires are anisotropic, showing the lowest flow resistance in the Z direction. HIC propagates in a plane perpendicular to that direction. Anisotropy was shown to be reduced by heat treatment processes.
- Flow resistance in the Z direction, nor any other, corresponds with the failure rate.
- For the flow resistance ratio, the Z/X correlation with the failure rate was found. It is interpreted that those ratios are a measure of microstructural damage caused by the cold rolling process.

BIBLIOGRAPHY

[1] American Petroleum Institute. May 2014. "Specification 17J Specification for Unbonded Flexible Pipe".

[2] P.F. Timmins. 1996. *Failure Control in Process Operations*. In: *ASM Handbook. Volume 19: Fatigue and Fracture*. Materials Park, Ohio: ASM International.

[3] M.C.E. Bandeira, R.M. Moreira, B. de Barros, R.C. Ribeiro, P. Silva, O.R. Mattos, F.P. dos Santos. 2019. "The Effect of H_2S Consumption on SSC Susceptibility of High Strength Wire Grades for Flexible Pipes". Corrosion 2019: NACE-2019-13483. Nashville, Tennessee.

[4] N. Desamais, C. Taravel-Condat. 2009. "On the Beneficial Influence of a Very Low Supply of H_2S on the Hydrogen Embrittlement Resistance of Carbon Steel Wires in Flexible Pipe Annulus". Offshore Technology Conference: OTC-19950-MS. Houston, Texas. DOI: 10.4043/19950-MS.

[5] A. Dugstad, S. Palencsár, L. Børvik, T. Berntsen. 2020. "Corrosion of Steel Armor Wires in Flexible Pipes – Effect of Small Amount of H_2S". Corrosion 2020: NACE-2020-14876.

[6] D. Lee, W.A. Backofen. 1966. "An Experimental Determination of the Yield Locus for Titanium and Titanium-Alloy Sheet (Yield Locus of Titanium and Titanium-Alloy Sheet under Combined-Stress Loading)". *Transactions of the Metallurgical Society of AIME* 236(7): 1077–1084.

[7] R.G. Wheeler, D.R. Ireland. 1966. "Multiaxial Plastic Flow of Zircaloy-2 Determined from Hardness Data". *Electrochemical Technology* 4: 313–317.

[8] D.R. Ireland. 1967. *Practical Technique for Obtaining and Using Plastic Anisotropy Information*. Technical report from 96th Annual Meeting of the American Institute of Mining, Metallurgical, and Petroleum Engineers. Los Angeles, California.

[9] S. Foissey, Ch. Bertout, X. Perroud. 2017. *Process for Manufacturing a Profiled Steel Wire*. Patent No. US 9,617,625 B2.

[10] K. Ankamma, D.V.V. Satyanarayana, G. Chandramohan Reddy, M. Komaraiah, N. Eswara Prasad. 2011. "In-Plane Anisotropy in Tensile Deformation and Its Influence on the Drawability of Nimonic c-263 Alloy Sheets". *Sadhana* 36: 223–249. DOI: 10.1007/s12046-011-0016-6.